



Spatiotemporal patterns of putaminal dopamine processing in Parkinson's disease: A multi-tracer positron emission tomography study

Jessie Fanglu Fu^{a,g,*}, Tilman Wegener^{a,d}, Ivan S. Klyuzhin^b, Julia G. Mannheim^{a,e,f}, Martin J. McKeown^{b,c}, A. Jon Stoessl^{b,c}, Vesna Sossi^{a,c}

^a Department of Physics and Astronomy, University of British Columbia, Vancouver, BC, Canada

^b Division of Neurology, Department of Medicine, University of British Columbia, Vancouver, BC, Canada

^c Djavad Mowafaghian Centre for Brain Health, Pacific Parkinson's Research Centre, University of British Columbia & Vancouver Coastal Health, Vancouver, BC, Canada

^d Department of Medical Engineering, University of Luebeck, Luebeck, Germany

^e Werner Siemens Imaging Center, Department of Preclinical Imaging and Radiopharmacy, Eberhard-Karls University Tuebingen, Tuebingen, Germany

^f Cluster of Excellence iFIT (EXC 2180) "Image Guided and Functionally Instructed Tumor Therapies", University of Tuebingen, Tuebingen, Germany

^g Athinoula A. Martinos Center for Biomedical Imaging, Massachusetts General Hospital, Charlestown, MA, USA

ARTICLE INFO

Keywords:

Parkinson's disease

PET

Striatal dopamine processing

Multivariate analysis

Spatiotemporal patterns

ABSTRACT

Alterations in different aspects of dopamine processing may exhibit different progressive behaviours throughout the course of Parkinson's disease. We used a novel data-driven multivariate approach to quantify and compare spatiotemporal patterns related to different aspects of dopamine processing from cross-sectional Parkinson's subjects obtained with: 1) 69 [¹¹C]±dihydrotetraabenazine (DTBZ) scans, most closely related to dopaminergic denervation; 2) 73 [¹¹C]d-*threo*-methylphenidate (MP) scans, marker of dopamine transporter density; 3) 50 6-[¹⁸F]fluoro-L-DOPA (FD) scans, marker of dopamine synthesis and storage. The anterior-posterior gradient in the putamen was identified as the most salient feature associated with disease progression, however the temporal progression of the spatial gradient was different for the three tracers. The expression of the anterior-posterior gradient was the highest for FD at disease onset compared to that of DTBZ and MP ($P = 0.018$ and $P = 0.047$ respectively), but decreased faster ($P = 0.006$) compared to that of DTBZ. The gradient expression for MP was initially similar but decreased faster ($P = 0.015$) compared to that for DTBZ. These results reflected unique temporal behaviours of regulatory mechanisms related to dopamine synthesis (FD) and reuptake (MP). While the relative early disease upregulation of dopamine synthesis in the anterior putamen prevalent likely extends to approximately 10 years after symptom onset, the presumed downregulation of dopamine transporter density may play a compensatory role in the prodromal/earliest disease stages only.

1. Introduction

In Parkinson's disease, motor dysfunction is traditionally associated with progressive loss of dopaminergic neurons in the substantia nigra and their projections to the striatum (Hirsch, 1994; Stoessl, 2012). Motor symptoms start to become clinically relevant when around 30–50 % of dopaminergic neurons are lost (Brooks, 2010). The loss of dopaminergic function follows a well characterized functional spatiotemporal pattern in which the dorsal posterior putamen contralateral to the more affected body side is affected first, followed by dopaminergic nerve terminal degeneration in the ventral and anterior putamen and the caudate nucleus. Previous studies showed that the disease may have

differential effects on various aspects of dopaminergic processing at different disease stages (Nandhagopal et al., 2009; Nandhagopal et al., 2011; Lee et al., 2000). These different aspects of dopaminergic function, including synthesis, storage, presynaptic reuptake, and turnover of dopamine, may exhibit different vulnerabilities to disease or potential compensatory responses, particularly in the early stage of the disease.

We have previously used positron emission tomography (PET) to quantify the different aspects of dopaminergic processing in Parkinson's disease subjects. In particular, we used 1) [¹¹C]±dihydrotetraabenazine (DTBZ), vesicular monoamine transporter type 2 (VMAT2) marker, to estimate dopamine vesicular uptake and storage; 2) [¹¹C]d-*threo*-methylphenidate (MP), dopamine transporter marker, to estimate

* Corresponding author at: Athinoula A. Martinos Center for Biomedical Imaging, 149 Thirteenth Street, Charlestown, MA 02129, USA.

E-mail address: flfu@mgh.harvard.edu (J.F. Fu).

<https://doi.org/10.1016/j.nicl.2022.103246>

Received 23 June 2022; Received in revised form 5 September 2022; Accepted 23 October 2022

Available online 25 October 2022

2213-1582/© 2022 The Authors. Published by Elsevier Inc. This is an open access article under the CC BY-NC-ND license (<http://creativecommons.org/licenses/by-nc-nd/4.0/>).

presynaptic dopamine reuptake capacity; 3) 6-[¹⁸F]-fluoro-L-DOPA (FD) to estimate dopamine synthesis and storage (Nandhagopal et al., 2009; Nandhagopal et al., 2011; Lee et al., 2000; Lee et al., 2004). By fitting exponential functions with pre-determined functional forms to the average putaminal binding/uptake values plotted as a function of disease duration for each tracer separately, FD uptake showed a faster decline until DTBZ binding decreased to less than 25 % of normal values, indicating upregulated FD uptake in early and mild disease stages. MP binding showed a similar progression rate as DTBZ binding throughout the course of the disease, but was lower than DTBZ binding in early disease. In more advanced disease, the progression rates appeared to be the same for all three tracers with the magnitudes ultimately converging to the same fraction of control values. As DTBZ binding is deemed to be the most direct measure of dopaminergic denervation (Borghet et al., 1995), the relative upregulation of dopamine synthesis and down-regulation of dopamine transporter density in early disease were interpreted to be of compensatory nature, with their breakdown contributing to the onset and progression of motor symptoms in more advanced disease (Nandhagopal et al., 2011; Lee et al., 2000). In addition, it was shown that even though the initial binding was higher for the anterior than the posterior putamen, the rate of decline may be the same for the anterior and posterior putamen for all three tracers (Nandhagopal et al., 2009; Lee et al., 2000, 2004). These observations suggested that mechanisms involved in disease progression have no or only minimal differential effect on the putaminal sub-regions.

Even though the previous studies examined the progressive changes in the dopaminergic system as evidenced by the three tracers, the univariate approach that was used suffered from possible limitations. First, the investigation was performed in pre-defined regions of interest (ROIs), which may oversimplify and restrict the assessment of the disease-induced changes. Second, the progressive change in the dopaminergic system was modelled by fitting exponential functions with pre-determined functional forms to the tracer binding values in each putaminal sub-region. This not only requires detailed and sometimes complicated parameter tuning, but also restricts the disease-related temporal changes to a fixed functional form. In contrast, we recently showed that a data-driven approach, the dynamic mode decomposition (DMD), was able to identify spatiotemporal patterns of dopaminergic denervation that are most sensitive to disease progression at the voxel level (Fu et al., 2020). Using DTBZ data, we demonstrated that the extracted spatiotemporal patterns of dopaminergic denervation were more sensitive to disease progression compared to results obtained by fitting exponential curves to the magnitude of binding/uptake values. In addition, we showed that DMD was able to decompose the overall progressive changes into distinct spatiotemporal patterns associated with different functional forms, thus presumably isolating different disease-related mechanisms.

In the present study, we extended DMD to extract features (i.e. spatiotemporal patterns) that are most sensitive to disease progression in three presynaptic dopaminergic targets. In addition, the comparison of the (\pm)DTBZ outcomes obtained in this study with those previously obtained in a different subject cohort with the (+)DTBZ enantiomer and a different scanner (Fu et al., 2020) indirectly served as a validation for the robustness of the findings obtained with the DMD approach. These new spatiotemporal patterns are expected to reflect more detailed and unique contributions from each aspect of dopaminergic processing to disease initiation, disease progression and potential compensatory mechanisms throughout the course of the disease, and thus complement and extend the findings obtained with the univariate results reported previously.

2. Methods and Materials

2.1. Study participants

This cross-sectional study included a total of 74 Parkinson's disease

subjects (disease duration: 0 to 26 years) previously reported in Nandhagopal et al. (2009, 2011) and 35 healthy controls age-matched to the Parkinson's subjects. Disease duration was estimated as the time from onset of motor symptoms. Parkinson's subjects were clinically assessed for motor functions using the motor segment of the Unified Parkinson's Disease Rating Scale (UPDRS-III) in the OFF-medication state. Detailed clinical characteristics are listed in Table 1. The study was approved by the Clinical Research Ethics Board of the University of British Columbia and all subjects provided informed written consent.

2.2. Scanning protocols

All PET scans were performed on the ECAT 953B tomograph (CTI Systems, Siemens, Knoxville, TN, USA) in 3D mode with a spatial resolution of approximately (8.5 mm)³. The scanning protocol and image reconstruction are described in detail elsewhere (Lee et al., 2000). Briefly, all Parkinson's subjects withdrew anti-parkinsonian medications for 12 h (immediate release levodopa) or 18–24 h (controlled release levodopa or dopamine agonists). Subjects were positioned using external lasers, and custom fitted thermoplastic masks were applied to minimize head movement. Intravenous injections of 202.4 \pm 32.1 MBq (\pm)DTBZ, 198.7 \pm 26.0 MBq MP and 185–260 MBq FD were accomplished over 60 s using an infusion pump (Harvard Instruments). PET scans were separated by at least 2.5 h following injection of ¹¹C tracers to allow for tracer decay. Acquired data were binned into 16 time frames for DTBZ and MP (4x1 min, 3x2 min, 8x5 min, 1x10 min) for a total of 60 min and 9 frames for FD (9x10 min) for a total of 90 min. Transmission scans required for attenuation correction were performed with external ⁶⁸Ge rods. PET images were reconstructed using filtered back-projection algorithm with a dimension of 128 \times 128 \times 31 and voxel size of 2.6078 \times 2.6078 \times 3.375 mm³. Data were corrected for decay, dead-time, normalization, attenuation, scattered and random coincidences. For each scan, the frames were spatially realigned with rigid-body transformation to minimize the impact of motion during the scan using Statistical Parametric Mapping (SPM, version 12, Wellcome Trust Centre for Neuroimaging, University College London, UK).

2.3. Image processing

After reconstruction, we first created a tracer-specific template in the ECAT-space (image dimension 128 \times 128 \times 31, voxel size 2.6078 \times 2.6078 \times 3.375 mm³) by realigning and averaging 20 healthy control subjects' images using the last 40 min for each tracer. All PET images were then registered to the tracer-specific healthy control template and parametric tracer binding images were generated for each tracer. In

Table 1

Clinical characteristics of the cross-sectional Parkinson's subjects. H&Y = Hoehn and Yahr scale. UPDRS-III = Unified Parkinson's Disease Rating Scale Part III. N/A = not applicable.

	Total #	Sex	Age (years)	Disease Duration (years)	H&Y	Total UPDRS-III
All Parkinson's subjects	74	55M/ 19F	60.4 \pm 7.5	7.55 \pm 5.98	1.75 \pm	27.9 \pm 11.8
DTBZ scans	69	51M/ 18F	60.5 \pm 10.5	7.38 \pm 5.69	1.71 \pm	27.3 \pm 10.9
MP scans	73	55M/ 18F	60.8 \pm 10.0	7.55 \pm 6.02	1.75 \pm	28.0 \pm 11.8
FD scans	50	36M/ 14F	60.3 \pm 11.0	7.41 \pm 6.08	1.68 \pm	26.6 \pm 11.4
Healthy controls	35	16M/ 19F	54.5 \pm 14.6	N/A	N/A	N/A

particular, parametric non-displaceable binding potential (BP_{ND}) images were generated for DTBZ and MP by the simplified reference tissue method (Wu and Carson, 2002) with the occipital cortex as the reference region, and parametric uptake rate constant (K_{OCC} , min^{-1}) images were generated for FD by the Patlak graphical method with the occipital cortex as the reference region (Patlak and Blasberg, 1985).

To further optimize the registration quality, we used a previously published two-step registration pipeline to bring all parametric ECAT images into a common Montreal Neurological Institute (MNI) space (Klyuzhin et al., 2018). In the first step, each of the three tracer-specific healthy control templates in ECAT-space (image dimension $128 \times 128 \times 31$, voxel size $2.6078 \times 2.6078 \times 3.375 \text{ mm}^3$) was registered to a common whole-brain template in MNI-space (image dimension $292 \times 193 \times 193$, voxel size $1 \times 1 \times 1 \text{ mm}^3$) with nearest neighbour interpolation and rigid and non-linear registration. The MNI whole-brain template mask was created with magnetic resonance (MR) defined segmentation using Freesurfer (Fischl et al., 2002). In the second step, the registered tracer-specific templates (in MNI space) were registered again to a putaminal template segmented using Freesurfer to further optimize the registration quality for the putamen. The resulting transformation matrix was saved and applied to the respective tracer binding images. The more and less affected hemispheres were defined in the transformed images as contralateral to the more and less clinically affected body sides (based on total UPDRS-III). Details about the putaminal template and the two-step registration pipeline can be found in Klyuzhin et al. (2018). An independent observer, blind to the analysis results, visually examined the registration quality for all images. The final analyses included 69 DTBZ scans, 73 MP scans and 50 FD scans. A total of 48 subjects had all three tracers images.

For comparison between results obtained with voxel-based DMD analysis and ROI analyses using data processed in identical way, manually defined circular ROI templates (7.8 mm in diameter) were created along the rostrocaudal axis without overlap for the anterior, middle and posterior putamen subregions and were placed on the parametric binding images in the MNI space to obtain the mean binding values in the three putaminal regions in the more and less affected sides separately for each tracer.

In order to compare the disease-related alterations in the data obtained with different PET tracers and correct for potential aging-related changes, standardized PET values were obtained at both ROI and voxel-level as the ratio between the tracer binding values and the mean age-matched normal values in the putamen as described previously (Nandhagopal et al., 2011). In short, aging-related changes were estimated using PET data from 35 healthy control subjects using linear mixed-effect models for each tracer. Linear relationships were obtained for each tracer for the mean putamen, which assumes the aging-related changes are uniform across the entire putamen. Expected aging-related binding values were estimated using the linear relationship for Parkinson's subjects. Voxel-wise standardized PET values in the putamen were obtained by dividing the parametric PET binding values by the corresponding expected aging-related binding values (constant over the whole putamen). Likewise, ROI-level standardized PET values were obtained by dividing the putaminal binding values by the corresponding expected aging-related binding values. Standardized PET values were used as inputs for both ROI-based and voxel-based DMD analyses.

2.4. Clinical characteristics

We applied one-way analysis of variance (ANOVA) to the age, disease duration, H&Y stages and UDPRS-III scores for Parkinson's subjects with DTBZ, MP and FD scans.

2.5. ROI-based analysis

To examine the relationship between the three PET tracers at different stages of disease, we applied one-way analysis of variance

(ANOVA) to the standardized PET values for DTBZ, MP and FD in the more and less affected anterior and posterior putamen separately in patients with early (<5 years of disease), mild (5–10 years of disease) and advanced (more than 10 years of disease) disease. False positive rates were controlled at $P = 0.05$ using Bonferroni-Holm's step-down procedure (Holm, 1979). The sample size for each disease stage is detailed in the [Supplementary Materials](#).

2.6. Voxel-based analysis – dynamic mode decomposition

We applied DMD to the parametric standardized values for Parkinson's subjects separately for each tracer ($N = 69$ for DTBZ, $N = 73$ for MP and $N = 50$ for FD) and also limited the analysis to data of Parkinson's subjects imaged with all three tracers ($N = 48$). Standardized PET values were used to remove the healthy aging effect in the derived spatiotemporal patterns. Mathematical details for the DMD pipeline were previously published (Fu et al., 2020). In brief, DMD decomposes the input parametric tracer binding images into spatial patterns of tracer binding values associated with orthogonal temporal progression curves in a data-driven fashion. These spatiotemporal patterns are by construct the imaging features most sensitive to disease progression.

As shown in Fig. 1, the input data X_t (standardized parametric tracer binding/uptake values) are first de-meaned along each column (subtract mean over all voxels) and then arranged so that the columns represent consecutive temporal snapshots of tracers' binding/uptake values at different disease duration values separated by Δt , thus representing the metric behaviour as a function of disease progression. In particular, for Parkinson's subjects, we used cross-sectional data of subjects with different disease duration to represent temporal snapshots of the metrics' values as a function of the disease course ($\Delta t = 1$ year). For time points with several snapshots (i.e. more than one subjects with the same disease duration), we used the average parametric images as a single input for the time point. DMD extracted spatial patterns of metrics' values and thus dopaminergic function (DMD modes, ϕ) associated with different temporal progression curves in the form $T(t) = \beta^* e^{\Omega t}$ where t is disease duration, β is the DMD amplitude (intercept at $t = 0$, corresponding to disease onset) and Ω is the decay constant. The DMD modes or spatial patterns consist of positive and negative voxel-weights for the PET standardized values in the putamen. The DMD amplitude β is the regression coefficient along each DMD mode that satisfies the linear equation $x_1 = \phi\beta$, where x_1 is the de-meaned data at the first time point ($t = 0$). The DMD amplitude thus represents the expression strength of the DMD mode at disease onset.

To determine if the temporal progression curves (both decay constants and DMD amplitudes) were different for the three different tracers, we randomly permuted the residuals of the DMD model to construct the 95 % confidence interval and the distributions of the differences in decay constants and DMD amplitudes between tracers. The P-value was calculated as the probability for the mean of the distributions of the group differences to be different from zero. The group difference was considered statistically significant for P-value < 0.05. Leave-one-out cross validation test was also performed on the temporal snapshots to examine the stability of the outputs. To compare the spatial patterns (DMD modes) obtained with the three tracers, we calculated R^2 for the voxel-wise spatial weights between each pair of tracers. No correction for multiple comparison was performed.

The robustness of the DMD method and the dependence of the results on image resolution was assessed by comparing the DMD results obtained with DTBZ with those obtained using the isomerically resolved (+)DTBZ and a different cohort of Parkinson's subjects scanned on a higher resolution scanner, the Siemens High Resolution Research Tomograph (HRRT, spatial resolution 2.5 mm^3)⁹. We performed correlation analyses on voxel weights for the first DMD spatial patterns and correlation analyses on the z-transformed temporal expressions of the first DMD spatial patterns obtained with two studies.

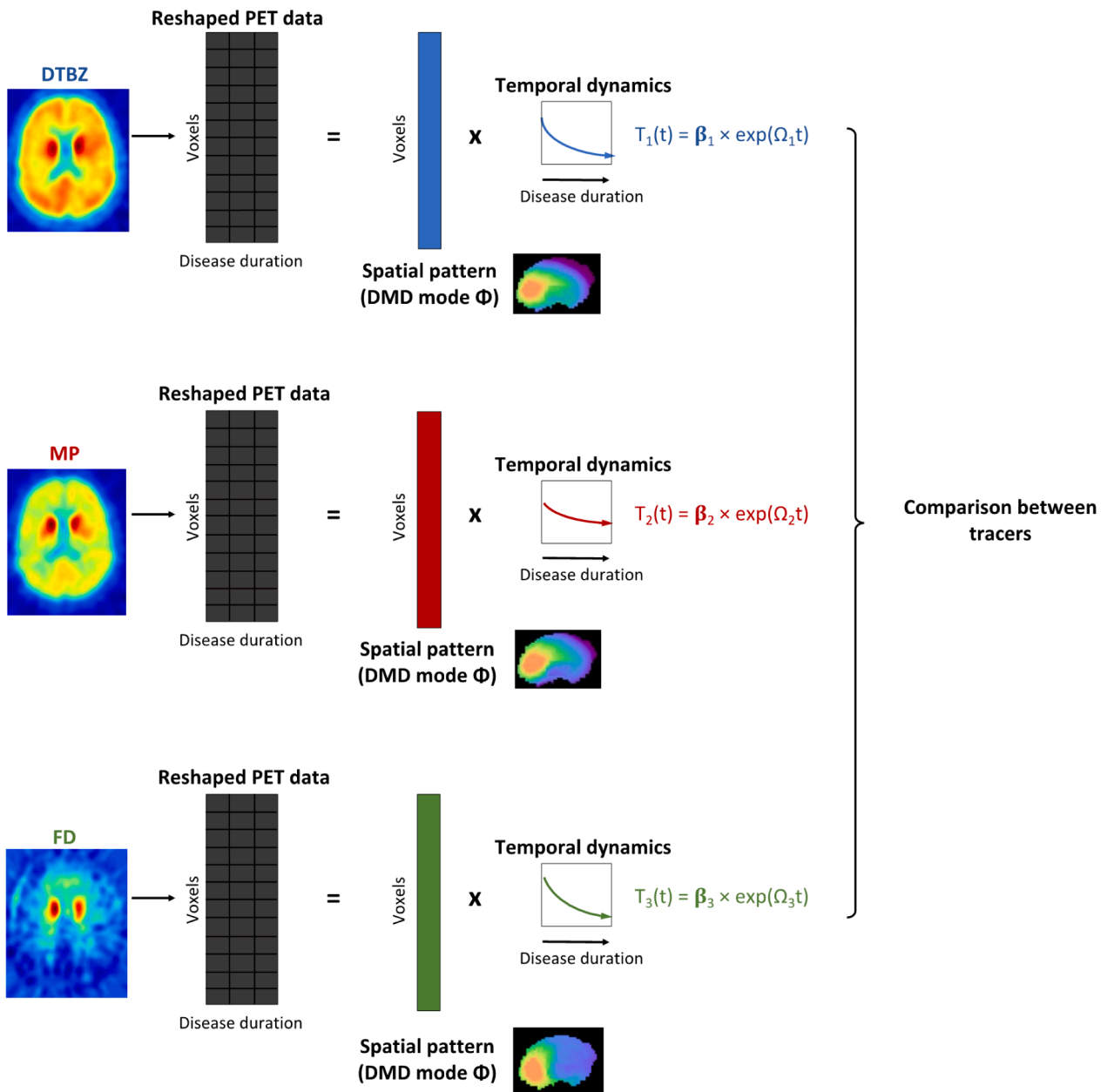


Fig. 1. Schematic diagram of the dynamic mode decomposition (DMD) approach. DTBZ = dihydrotetrabenazine. FD = fluoro-L-DOPA. MP = d-threo-methylphenidate. PET = positron emission tomography.

2.7. Univariate analysis

To compare the DMD results with univariate analyses results, we fitted exponential functions (in the form $y = \beta_1 e^{-\beta_2 t}$) to the standardized PET values as a function of disease duration in the anterior, middle and posterior putamen for the three PET tracers.

All codes were written in Matlab and are available upon direct request to the corresponding author, however PET data used in this study cannot be made available publicly in order to protect patient confidentiality.

3. Results

There was no significant difference in clinical characteristics between the subjects with DTBZ, MP and FD scans.

3.1. ROI-based analysis

In early disease (disease duration < 5 years), FD showed significantly higher standardized values than DTBZ and MP in the more ($P < 0.01$ for DTBZ, $P < 0.05$ for MP, corrected) and less ($P < 0.001$ for DTBZ, $P < 0.01$ for MP, corrected) affected anterior putamen. In the posterior putamen, standardized FD values were significantly higher than those of MP in both the more ($P < 0.01$, corrected) and less affected sides ($P < 0.05$, corrected), but not DTBZ (Fig. 2). There was no significant difference in the standardized PET values between DTBZ and MP. In mild to advanced disease, there were no significant group differences in the standardized PET values between any of the tracers after correction for multiple comparison.

3.2. Voxel-based analysis – dynamic mode decomposition

DMD outputs obtained using all Parkinson's subjects and using only

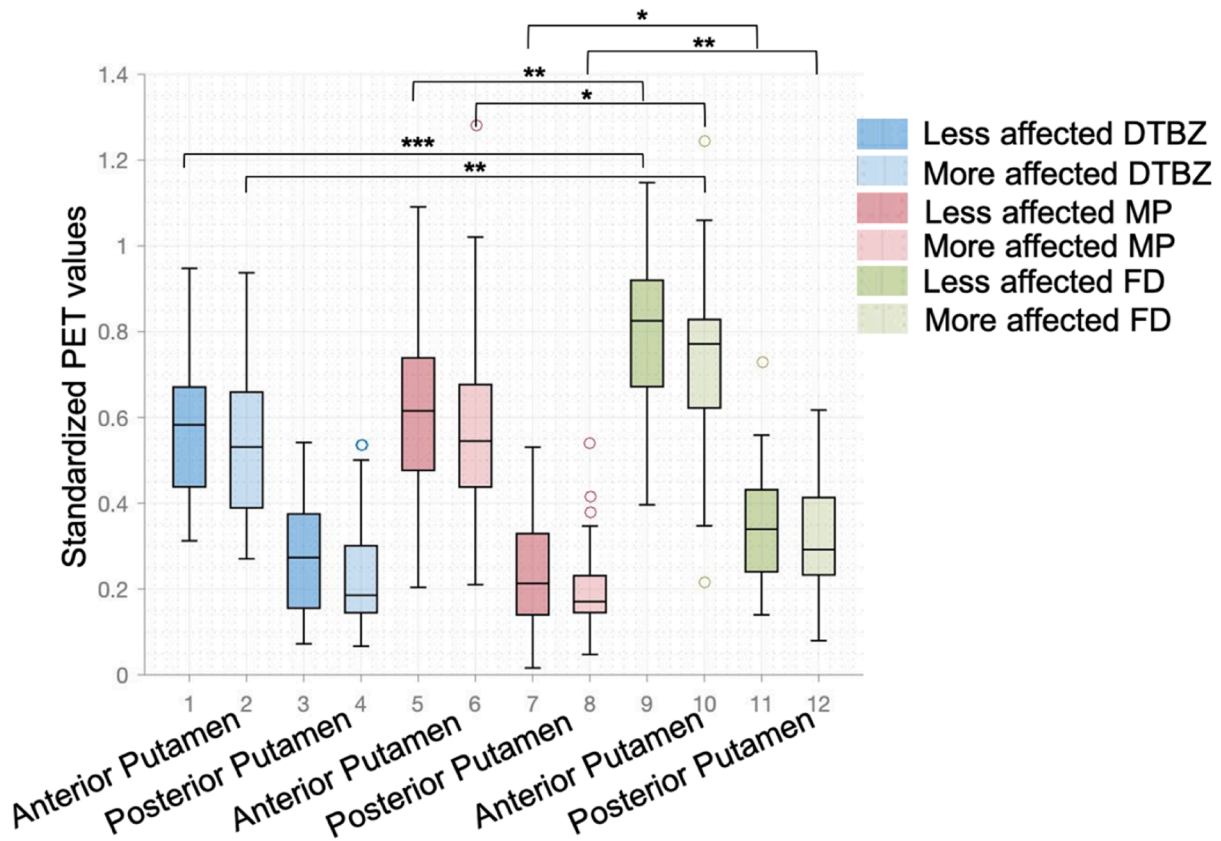


Fig. 2. Standardized PET values for DTBZ, MP and FD in the less and more affected anterior and posterior putamen in early disease (disease duration less than 5 years). The standardized PET values were derived as the tracer binding values (BP_{ND} for DTBZ and MP and K_{occ} for FD) normalized by the age-matched normal values. One-way analysis of variance was used to examine the differences between tracers. * = P-value < 0.05. ** = P-value < 0.01. *** = P-value < 0.001. DTBZ = dihydrotetabenazine. FD = fluoro-L-DOPA. MP = d-threo-methylphenidate. PET = positron emission tomography.

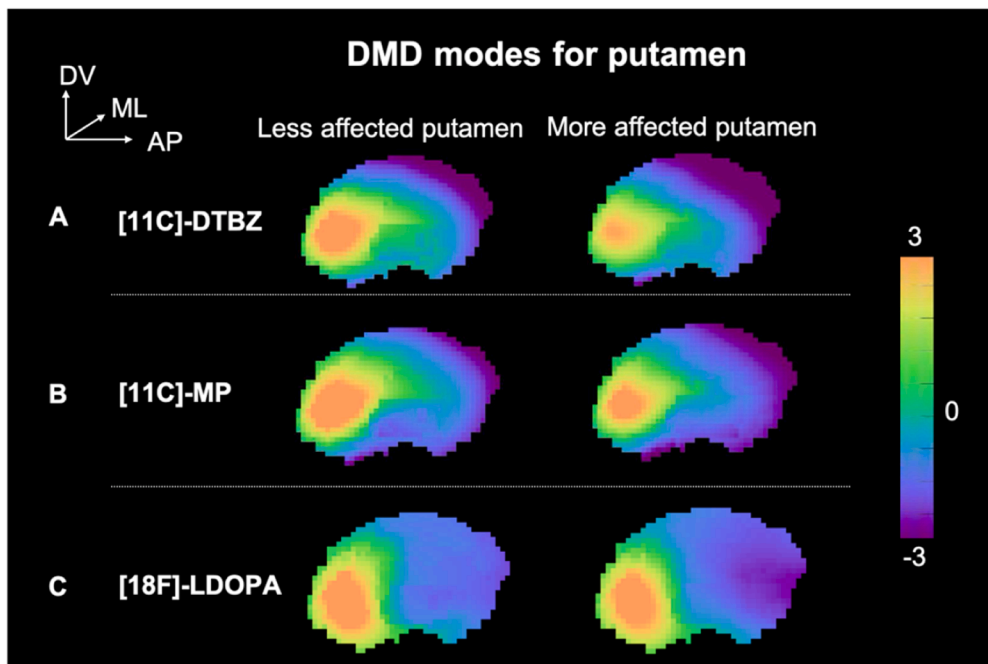


Fig. 3. Dynamic mode decomposition (DMD) modes/spatial patterns (z-transformed) in the less and more affected putamen for (A) DTBZ, (B) MP and (C) FD. DTBZ = dihydrotetabenazine. FD = fluoro-L-DOPA. MP = d-threo-methylphenidate. DV = dorsal-ventral. ML = Medial-lateral. AP = anterior-posterior.

subjects with all three scans were almost identical (less than 8 % differences in the estimation of decay constant and DMD amplitudes for all tracers). Therefore, only DMD outputs obtained with all subjects are shown and discussed in the main manuscript. DMD outputs obtained with subjects with all three PET tracers can be found in the [Supplementary Materials](#).

DMD extracted one spatiotemporal pattern accounting for 89 %, 86 % and 84 % of the total variance in DTBZ, MP and FD data respectively. DMD identified the characteristic gradients consisting of increasingly positive weights in the anterior putamen and increasingly negative weights in the posterior putamen in both the more and less affected putamen as the feature most sensitive to disease progression in all three tracers (Fig. 3). Voxel-wise comparison showed high similarity in the spatial patterns obtained with the three tracers (Table 2), and a more detailed comparison is included in the [Supplementary Materials](#). Visually, DTBZ and MP showed a clear asymmetry between the more and less affected sides with the anterior-posterior gradient being more prominent in the less affected side; FD, on the other hand, did not show obvious asymmetry. Applying DMD to the less and more affected sides separately gave similar results as applying DMD to both sides together, we therefore focused on the results obtained with using both sides together to reduce the number of comparisons.

Temporal expressions of the anterior-posterior gradients decreased gradually with disease duration for all tracers (Fig. 4). FD showed a significantly higher initial expression (DMD amplitude) of the gradient compared to DTBZ ($P = 0.018$) and MP ($P = 0.047$) (Table 2); no significant difference was observed between DTBZ and MP. DTBZ showed a significantly lower decay constant (decline rate) for the expression of the anterior-posterior gradient compared to both MP ($P = 0.015$) and FD ($P = 0.006$); no significant difference in the decay constants was observed between MP and FD (Table 2). Error bars obtained with cross-validation tests were small as shown in Fig. 4, indicating the robustness of the DMD outputs.

The DMD spatial patterns ($R^2 = 0.64$) and the temporal progression curves ($P = 10^{-15}$, $R^2 = 0.99$) obtained with independent subject cohorts scanned on ECAT (this study) and HRRT (previous study⁹) were highly correlated. A detailed comparison is included in the [Supplementary Materials](#).

3.3. Univariate analysis

Univariate results were consistent with the DMD results in terms of the relationship between the three tracers. Detailed univariate results can be found in the [Supplementary Materials](#).

4. Discussion

In this study, we used a novel data-driven multivariate approach to

Table 2

Dynamic mode decomposition (DMD) outputs obtained with the three PET tracers. R^2 is the voxel-wise correlation value for the DMD spatial patterns. P-values for decay constants and DMD amplitudes were obtained using random permutation tests. DTBZ = dihydrotetabenazine. FD = fluoro-L-DOPA. MP = d-threo-methylphenidate. PET = positron emission tomography. N/A = not applicable.

	DTBZ	MP	FD	DTBZ vs MP	DTBZ vs FD	MP vs FD
Spatial pattern	N/A	N/A	N/A	$R^2 = 0.85$	$R^2 = 0.66$	$R^2 = 0.59$
Decay constant (ϕ)	-0.0248	-0.0706	-0.0758	$P = 0.015$	$P = 0.006$	$P = 0.39$
DMD amplitude (β)	16.3	16.7	27.7	$P = 0.49$	$P = 0.018$	$P = 0.047$

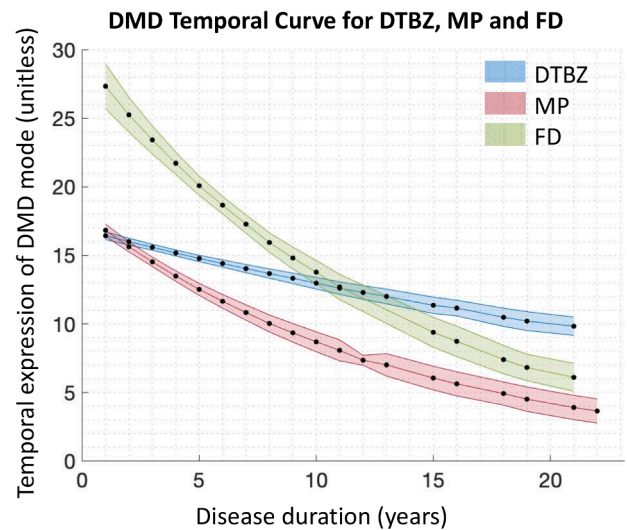


Fig. 4. Dynamic mode decomposition (DMD) temporal progression (unitless) curves for DTBZ, MP and FD, associated with the anterior-posterior gradient in the putamen (DMD modes shown in Fig. 3). Error bars of the temporal progression curves were obtained using cross-validation. DTBZ = dihydrotetabenazine. FD = fluoro-L-DOPA. MP = d-threo-methylphenidate.

quantify and compare the spatiotemporal patterns of progressive alterations in several aspects of the dopaminergic system in Parkinson's disease. While overall consistent with previous findings, the novel data-driven approach revealed additional information on the temporal relationships between the three aspects of dopaminergic system.

4.1. Comparing with previously reported DMD results

The spatiotemporal pattern obtained with DTBZ was similar to the previous spatiotemporal pattern reported with a different Parkinson's cohort on a PET scanner with higher spatial resolution and (+)DTBZ (Fu et al., 2020). Notably, both studies identified the anterior-posterior gradient as the dominant progression-related feature in dopaminergic denervation and showed that the expression of the gradient decreased gradually as disease progresses. This comparison demonstrates the applicability and robustness of the DMD approach and shows that the lower resolution of the ECAT scanner did not hamper the analysis. However, previous DMD results obtained with the HRRT scanner also showed a second spatiotemporal pattern consisting of a dorsal-ventral gradient in the putamen. The absence of a second spatiotemporal pattern in this study was likely due to the use of (\pm)DTBZ tracer and the lower resolution of the ECAT scanner.

4.2. DMD modes (anterior-posterior gradients in the putamen)

Previous studies conducted on a similar subject cohort (Nandhagopal et al., 2011; Lee et al., 2000) investigated the temporal progression of pre-defined spatial regions using a univariate approach. In contrast, this study used a data-driven approach to identify spatiotemporal patterns that are most sensitive to disease progression for three presynaptic dopaminergic tracers at a voxel-level. The strong expression of the anterior-posterior gradient at disease onset is consistent with the evidence that disease has initially a differential effect on putaminal sub-regions rather than an uniform impact on the entire structure, and that such pattern originates already in the prodromal stage. Analyzing subjects in the prodromal stage (e.g. carriers of mutations that increase the risk of Parkinson's disease) is needed to fully understand the factors responsible for disease initiation.

For all three tracers, the anterior-posterior gradient was identified as the salient and only spatial pattern related to disease progression, with

its strength decreasing over time, even though previous univariate analyses showed that the anterior-posterior gradient was maintained throughout the course of the disease for all three tracers (Nandhagopal et al., 2009; Lee et al., 2004). These findings suggest that after clinical disease is present, mechanisms responsible for disease progression might also have a differential impact on the putaminal sub-regions and these mechanisms can be further broken down into the ones responsible for dopamine denervation and potential regulatory changes by comparing the temporal curves of the three imaging targets. The lack of differential progression rates for the anterior and posterior putamen in the univariate analysis is likely due to the higher sensitivity of the DMD approach to extract spatial features that are most sensitive to disease progression by construct, compared to fitting the data with pre-defined models, which are often highly influenced by the number of parameters, parameter tuning and noise.

4.3. DMD temporal expressions

The expression of the anterior-posterior gradient obtained with DTBZ had the slowest decay rate compared to that of MP and FD. VMAT2 density (estimated by DTBZ) is deemed a reasonably direct measure of the degree of dopaminergic terminal denervation and is the least sensitive to disease-related regulatory changes comparing to MP and FD (Borghet et al., 1995; Fu et al., 2019), even though VMAT2 expression on non-dopaminergic terminals may not be negligible in advanced disease (see Limitations). MP and FD bindings reflect both dopaminergic terminal degeneration and disease-related regulatory changes (Nandhagopal et al., 2011; Lee et al., 2000; Afonso-Oramas et al., 2010; Neff and Hadjiconstantinou, 1995). The strongest expression of the FD spatial gradient at disease onset likely reflects an upregulation of dopamine synthesis in the surviving terminals; here found to be most strongly present in the anterior putamen. While this was already inferred from the univariate analysis in early disease, this voxel-based data driven approach provides additional information about the progressive behaviours of such regulatory changes. The relatively rapid decline of the expression strength of the FD pattern compared to the DTBZ pattern can be interpreted as a decline of the compensatory upregulation of dopamine synthesis. Indeed, after approximately 10 years of disease, the expression of the gradient becomes lower for FD compared to DTBZ, suggesting that while the gradient of dopaminergic terminal loss is relatively constant throughout the course of disease, the compensatory responses in dopamine synthesis persist in early disease but eventually break down as the degree of dopaminergic degeneration increases.

In this study, we did not observe any significant difference between DTBZ and MP binding at any disease stage using univariate analysis contrary to previous results (Lee et al., 2000). This is likely due to the differences in preprocessing pipelines: 1) voxel-level analyses require normalization of all images onto a common space, 2) the use of more standardized ROI template compared to previously manually placed ROIs, 3) the addition of frame-to-frame realignment which was not used in previous studies. In addition, the current study includes fewer subjects compared to previous studies due to the more demanding preprocessing pipeline (Nandhagopal et al., 2011; Lee et al., 2000). On the other hand, with the voxel-based analysis, we observed that the expression of the anterior-posterior gradient in MP was initially similar but decreased faster compared to that of DTBZ and decreased at a rate similar to FD. Extrapolating the MP temporal curve before $t = 0$ shows the expression of the anterior-posterior gradient is higher for MP than DTBZ in the prodromal stage. This observation together with the significantly reduced MP binding in both asymptomatic leucine-rich repeat kinase 2 (LRRK2) mutation carriers (with higher risks of developing Parkinson's disease) and in early Parkinson's subjects compared to healthy controls (Nandhagopal et al., 2011; Lee et al., 2000; Nandhagopal et al., 2008; Wile et al., 2017) support the hypothesis that the downregulation of dopamine transporter density in the posterior

putamen may be due to a compensatory mechanism particularly relevant in the prodromal stage. It is possible to speculate that the breakdown of this compensatory effect may play an important role in the clinical onset of the disease. In addition, the decay rates for the temporal curves of both MP and FD were similar, suggesting the underlying mechanisms responsible for the breakdown of the compensatory responses from dopamine synthesis and dopamine transporters may be similar, but occurring at different stages of the disease.

4.4. Unique strengths of DMD

A unique strength of the DMD approach is that it is completely data driven thus eliminating a potential bias arising from an a-priori hypothesis about the image feature most sensitive to disease progression. This ensures that the finding of similar and yet not identical spatio-temporal patterns most closely related to disease progression reflects objective and most relevant information contained in the data. The DMD approach revealed unique longitudinal behaviours of the three presynaptic dopaminergic imaging targets: 1) differential progression rates for the anterior and posterior putamen, which were not differentiable with univariate analyses, 2) different progression rates for the anterior-posterior pattern for FD and MP compared to DTBZ even in advanced disease, which were again not differentiable in advanced disease stage with univariate analyses, 3) similar progression rates for the anterior-posterior pattern for FD and MP. As a minor note, these results could also inform on tracer-specific markers that are most sensitive for disease detection. For example, while a ratio between PET binding values in the anterior and posterior putamen may be a good disease detection marker when FD is used, an overall decline in putaminal binding values compared to controls may be a more sensitive disease detection marker for DTBZ.

4.5. Limitations

There are possible confounds and limitations to these interpretations. For example, VMAT2 is also present in other monoaminergic terminals (e.g., serotonin and noradrenaline) in the striatum and their contribution to DTBZ binding in more advanced disease may not be negligible, which may bias the interpretation of the observed DTBZ anterior-posterior gradient. VMAT2 binding to non-dopaminergic monoaminergic terminals may also impact the ability for DTBZ to serve as a benchmark for dopaminergic integrity; however, comparing to FD and MP, DTBZ binding is more directly correlated with dopaminergic terminal density for the purpose of this study. Similarly, FD uptake also reflects dopamine synthesis in other monoaminergic neurons (e.g. the serotonergic neurons) (Pavese et al., 2012). The lower expression of the anterior-posterior gradient in advanced disease in FD may partially reflect the relatively higher proportion of dopamine synthesized by non-dopaminergic neurons in the posterior putamen (Pavese et al., 2012). Even though DAT is selectively expressed on dopaminergic neurons, MP binding is also affected by other factors such as binding to non-dopaminergic neurons (e.g., noradrenergic) and occupancy of the dopamine transporter by synaptic dopamine. While we need to be cautious when interpreting these results, the presence of such binding sources may have a larger effect in non-striatal regions compared to the putamen (Pavese et al., 2012). Other limitations include the use of cross-sectional data to model disease progression, for which individual subject variability could represent a potential confounding factor. Previous studies, however, showed very similar disease progression curves obtained with cross-sectional data alone (Lee et al., 2000, 2004) and with a combination of cross-sectional and longitudinal data (Nandhagopal et al., 2009, 2011). Inclusion of longitudinal data in the current analysis did not change the results (Supplementary Materials). Using data from all three tracers for all the subjects also did not impact the results (Supplementary Materials). This is expected as we demonstrated that the results of the DMD analysis performed on two completely different

subject cohorts using two different scanners were very similar. Lastly, there is potential floor effect of dopamine function in the posterior putamen already in the early disease stages, which could affect the temporal behaviour of the expression of the anterior-posterior gradient. However, the floor effect due to dopamine denervation is mainly reflected by DTBZ data, which showed a relatively well-maintained anterior-posterior gradient in the putamen throughout the course of the disease. Therefore, the faster decline rates of the expression of the anterior-posterior gradient observed in MP and FD are unlikely due to floor effect alone.

5. Conclusion

In this work, we applied a novel, completely data-driven multivariate approach to identify spatiotemporal patterns of progressive alterations in several aspects of the dopaminergic system in Parkinson's disease. In all cases, a putaminal anterior-posterior gradient was identified as the only salient feature most sensitive to disease progression, indicating similar topological behaviour of the three targets under investigation. In addition to a spatially characterized relative upregulation of dopamine synthesis in early to mild disease, overall consistent with previous findings, our results provided new insights on the disease-induced progressive changes of dopamine synthesis and reuptake which differ from those observed for dopaminergic denervation. More specifically, our results suggest that while downregulation of dopamine transporter density may be preferentially compensatory in the prodromal stage, the breakdown of its compensatory effects may be related to disease onset. On the other hand, the potential compensatory effects from upregulation of dopamine synthesis, mostly found in the anterior putamen, may persist until a more advanced disease stage.

Declaration of Competing Interest

The authors declare that they have no known competing financial interests or personal relationships that could have appeared to influence the work reported in this paper.

Data availability

All codes are available upon direct request to the corresponding author, however PET data used in this study cannot be made available publicly in order to protect patient confidentiality.

Acknowledgements

The study was financially supported by the Natural Sciences and Engineering Research Council of Canada (NSERC) (grant number 240670-13), Brain Canada (grant number 64457), and Canadian Institutes of Health Research (CIHR) (grant number 125989). AJS is supported by the Canada Research Chairs program. JF receives scholarship funding from the Isotopes for Science and Medicine program (NSERC-CREATE). TRIUMF is supported by NRC. TW is supported by ENEN + project (EURATOM research and training Work Programme 2016-2017 (1#755576)) and the PROMOS Study or Internship Abroad Scholarships (German Academic Exchange Service (DAAD)).

Author Contribution Statement

VS and AJS designed the study. TW, IK, JM and JF contributed to data preprocessing. JF, MM and TW contributed to the data analysis pipeline. JF and TW were responsible for the data analysis and preparation of the results. JF and VS contributed to the design and draft of the manuscript. AJS, MM, IK, TW, JM gave critical comments on the manuscript. All the authors read and gave final approval of the

manuscript to be published.

Appendix A. Supplementary data

Supplementary data to this article can be found online at <https://doi.org/10.1016/j.nicl.2022.103246>.

References

- Afonso-Oramas, D., Cruz-Muros, I., Barroso-Chinea, P., de la Rosa, D.Á., Castro-Hernández, J., Salas-Hernández, J., Giráldez, T., González-Hernández, T., 2010. The dopamine transporter is differentially regulated after dopaminergic lesion. *Neurobiol. Dis.* 40 (3), 518–530.
- Borghet, T.V., Kilbourn, M., Desmond, T., Kuhl, D., Frey, K., 1995. The vesicular monoamine transporter is not regulated by dopaminergic drug treatments. *Eur. J. Pharmacol.* 294 (2-3), 577–583.
- Brooks, D.J., 2010. Imaging dopamine transporters in Parkinson's disease. *Biomark. Med.* 4 (5), 651–660.
- Fischl, B., Salat, D.H., Busa, E., Albert, M., Dieterich, M., Haselgrove, C., van der Kouwe, A., Killiany, R., Kennedy, D., Klaveness, S., Montillo, A., Makris, N., Rosen, B., Dale, A.M., 2002. Whole brain segmentation: Automated labeling of neuroanatomical structures in the human brain. *Neuron* 33 (3), 341–355.
- Fu, J.F., Klyuzhin, I., McKenzie, J., Neilson, N., Shahinfard, E., Dinelle, K., McKeown, M. J., Stoessl, A.J., Sossi, V., 2019. Joint pattern analysis applied to PET DAT and VMAT2 imaging reveals new insights into Parkinson's disease induced presynaptic alterations. *NeuroImage Clin.* 23, 101856.
- Fu, J.F., Klyuzhin, I.S., McKeown, M.J., Stoessl, A.J., Sossi, V., 2020. Novel data-driven, equation-free method captures spatio-temporal patterns of neurodegeneration in Parkinson's disease: Application of dynamic mode decomposition to PET. *NeuroImage Clin.* 25, 102150.
- Hirsch, E.C., 1994. Biochemistry of Parkinson's disease with special reference to the dopaminergic systems. *Mol. Neurobiol.* 9 (1-3), 135–142.
- Holm, S., 1979. A simple sequentially rejective multiple test procedure A simple sequentially rejective multiple test procedure. *Source Scand. J. Stat. Scand. J. Stat.* 6, 65–70.
- Klyuzhin, I.S., Fu, J.F., Hong, A., Sacheli, M., Shenkov, N., Matarazzo, M., Rahmim, A., Stoessl, A.J., Sossi, V., Chen, K., 2018. Data-driven, voxel-based analysis of brain PET images: Application of PCA and LASSO methods to visualize and quantify patterns of neurodegeneration. *PLoS ONE* 13 (11), e0206607.
- Lee, C.S., Samii, A., Sossi, V., Ruth, T.J., Schulzer, M., Holden, J.E., Wudel, J., Pal, P.K., De La Fuente-Fernandez, R., Calne, D.B., Stoessl, A.J., 2000. In vivo positron emission tomographic evidence for compensatory changes in presynaptic dopaminergic nerve terminals in Parkinson's disease. *Ann. Neurol.* 47 (4), 493–503.
- Lee, C.S., Schulzer, M., de la Fuente-Fernández, R., Mak, E., Kuramoto, L., Sossi, V., Ruth, T.J., Calne, D.B., Stoessl, A.J., 2004. Lack of regional selectivity during the progression of Parkinson disease: Implications for pathogenesis. *Arch. Neurol.* 61 (12), 1920–1925.
- Nandhagopal, R., Mak, E., Schulzer, M., McKenzie, J., McCormick, S., Sossi, V., Ruth, T. J., Strongosky, A., Farrer, M.J., Wszolek, Z.K., Stoessl, A.J., 2008. Progression of dopaminergic dysfunction in a LRRK2 kindred: a multitracer PET study. *Neurology* 71 (22), 1790–1795.
- Nandhagopal, R., Kuramoto, L., Schulzer, M., Mak, E., Cragg, J., Lee, C.S., McKenzie, J., McCormick, S., Samii, A., Troiano, A., Ruth, T.J., Sossi, V., de la Fuente-Fernandez, R., Calne, D.B., Stoessl, A.J., 2009. Longitudinal progression of sporadic Parkinson's disease: A multi-tracer positron emission tomography study. *Brain* 132 (11), 2970–2979.
- Nandhagopal, R., Kuramoto, L., Schulzer, M., Mak, E., Cragg, J., McKenzie, J., McCormick, S., Ruth, T.J., Sossi, V., de la Fuente-Fernandez, R., Stoessl, A.J., 2011. Longitudinal evolution of compensatory changes in striatal dopamine processing in Parkinson's disease. *Brain* 134 (11), 3290–3298.
- Neff, N.H., Hadjicostantinou, M., 1995. Aromatic L-amino acid decarboxylase modulation and Parkinson's disease. *Prog. Brain Res.* 106, 91–97.
- Patlak, C.S., Blasberg, R.G., 1985. Graphical evaluation of blood-to-brain transfer constants from multiple-time uptake data. Generalizations. *J. Cereb. Blood Flow Metab.* 5 (4), 584–590.
- Pavese, N., Simpson, B.S., Metta, V., Ramlackhansingh, A., Chaudhuri, K.R., Brooks, D.J., 2012. [18F]FDOPA uptake in the raphe nuclei complex reflects serotonin transporter availability. A combined [18F]FDOPA and [11C]DASB PET study in Parkinson's disease. *NeuroImage* 59 (2), 1080–1084.
- Stoessl, A.J., 2012. Neuroimaging in Parkinson's disease: from pathology to diagnosis. *Parkinsonism Relat. Disord.* 18 (Suppl 1), S55–S59.
- Wile, D.J., Agarwal, P.A., Schulzer, M., Mak, E., Dinelle, K., Shahinfard, E., Vafai, N., Hasegawa, K., Zhang, J., McKenzie, J., Neilson, N., Strongosky, A., Uitti, R.J., Guttman, M., Zabetian, C.P., Ding, Y.-S., Adam, M., Aasly, J., Wszolek, Z.K., Farrer, M., Sossi, V., Stoessl, A.J., 2017. Serotonin and dopamine transporter PET changes in the premotor phase of LRRK2 parkinsonism: cross-sectional studies. *Lancet Neurol.* 16 (5), 351–359.
- Wu, Y., Carson, R.E., 2002. Noise reduction in the simplified reference tissue model for neuroreceptor functional imaging. *J. Cereb. Blood Flow Metab.* 22 (12), 1440–1452.